

A unifying theory of branching morphogenesis

Edouard Hannezo^{1,2,3,8,9}, Colinda L. G. J. Scheele^{4,8}, Mohammad Moad⁵, Nicholas Drogo⁶,
Rakesh Heer⁵, Rosemary V. Sampogna⁷, Jacco van Rheenen^{4,9} and Benjamin D.
Simons^{1,2,3,9,10}

¹*Cavendish Laboratory, Department of Physics, University of Cambridge, Cambridge, CB3
0HEUK*

²*The Wellcome Trust/Cancer Research UK Gurdon Institute, University of Cambridge,
Cambridge, CB2 1QN, UK*

³*The Wellcome Trust/Medical Research Council Stem Cell Institute, University of Cambridge,
CB2 1QN, UK*

⁴*Cancer Genomics Netherlands, Hubrecht Institute-KNAW and University Medical Centre
Utrecht, Utrecht, 3584CT, The Netherlands*

⁵*1 Northern Institute for Cancer Research, Newcastle University, Newcastle upon Tyne NE2
4AD, UK*

⁶*University of Rochester, Department of Biomedical Engineering, 500 Joseph C. Wilson Blvd,
Rochester, NY, 14627, USA*

⁷*Division of Nephrology, Department of Medicine, Columbia University College of Physicians
and Surgeons, New York, NY, 10032, USA*

⁸*These authors contributed equally*

⁹*Co-corresponding author*

¹⁰*Lead contact: bds10@cam.ac.uk*

⁹*Correspondence: edouard.hannezo@ist.ac.at, j.vanrheenen@hubrecht.eu, bds10@cam.ac.uk*

Summary

The morphogenesis of branched organs remains a subject of abiding interest. Although much is known about the underlying signaling pathways, it remains unclear how macroscopic features of branched organs, including their size, network topology and spatial patterning, are encoded. Here we show that, in mouse mammary gland, kidney and human prostate, these features can be explained quantitatively within a single unifying framework of branching and annihilating random walks. Based on quantitative analyses of large-scale organ reconstructions and proliferation kinetics measurements, we propose that morphogenesis follows from the proliferative activity of equipotent tips that stochastically branch and randomly explore their environment, but compete neutrally for space, becoming proliferatively inactive when in proximity with neighboring ducts. These results show that complex branched epithelial structures in mammalian tissues develop as a self-organized process, reliant upon a strikingly simple, but generic, rule, without recourse to a rigid and deterministic sequence of genetically programmed events.

Keywords

Branching morphogenesis; Mammary gland; Kidney; Prostate; Mathematical modelling; Branching and Annihilating Random Walks; Out-of-equilibrium processes; Self-organisation

Introduction

Branching morphogenesis has fascinated biologists and mathematicians for centuries, both because of its complexity and ubiquity (Hogan, 1999; Lu and Werb, 2008; Metzger et al., 2008; Iber and Menshykau, 2013). In higher organisms, many organs are organized into ductal tree-like structures comprising tens of thousands of branches, which typically function to maximize the surface of exchange between the epithelium and its lumen. Examples include lung, kidney, prostate, liver, pancreas, the circulatory system and the mammary gland epithelium. Alongside

metazoa, tree crowns and root systems as well as coral reefs often display a similar branched organization (Harrison, 2010) raising the question of whether common mechanisms could underlie their formation. Extensive investigations have identified features shared by all branched organs, which are formed by repeated cycles of branching (either through side-branching or tip-splitting), together with phases of ductal elongation (Iber and Menshykau, 2013).

Attempts to resolve the regulatory basis of branching morphogenesis have been targeted at different length scales, offering contrasting perspectives: First, at the molecular scale, key regulatory signaling pathways, for instance controlling proliferation, have been resolved in multiple organs (Iber and Menshykau, 2013). Second, at the cellular and mesoscopic scale, measurements of gene expression patterns and branching shape have implicated Turing-like mechanisms in the regulation of the first rounds of repetitive branching in the lung (Miura, 2008) and kidney (Menshykau and Iber, 2013), as well as explaining the relative importance of side-branching and tip-splitting in different organs (Guo et al., 2014). Alternative, potentially overlapping, explanations based on mechanical (Gjorevski and Nelson, 2011) or viscous (Lubkin and Murray, 1995) models have been proposed, although direct *in vivo* confirmation is still lacking. However, oriented cell divisions (Yu et al., 2009), collective cell migration (Huebner et al., 2016; Riccio et al., 2016) and cytoskeleton-driven cell shape changes (Elliott et al., 2015; Kim et al., 2015) have all been shown to play a role. Yet, even a perfect understanding of how single branching events occur would not explain how thousands of tips and branches become coordinated at the organ scale, to specify a complex ductal network.

Therefore, here, we adopt an alternative “non-reductionist” approach, and test whether the statistical properties of branched networks can be predicted without extensively addressing the detailed underlying molecular and cellular regulatory processes. Historically, the development of such statistical approaches has been limited by the lack of high resolution biological data on the complete organ structure. However, this problem is becoming alleviated by advances in imaging techniques (Metzger et al., 2008; Sampogna et al., 2015; Short et al., 2014), which provide an

ideal platform to question how a complex 3D organ structure is encoded. Does it form from the unfolding of an intrinsic deterministic program or is it shaped by extrinsic influences and stochastic processes?

In the following, we use detailed whole-organ imaging and 3D reconstructions of the mouse mammary gland epithelium, mouse kidney and human prostate to address the spatiotemporal dynamics of branching morphogenesis. We show that the detailed statistical properties of these organs share key underlying features, which can be explained quantitatively through a remarkably simple and conserved design principle, based on the theory of branching and annihilating random walks (BARWs). In this model, growing ductal tips follow the same, time-invariant, statistical rules based on stochastic ductal branching and random exploration of space. However, when an active tip comes into proximity with a neighboring duct, it becomes irreversibly inactive (differentiating and exiting cell cycle), leading to the termination of the duct. We show that, together, these simple local rules are enough to allow the epithelium to grow in a self-organized manner, into a complex ductal network with conserved statistical properties that are quantitatively predicted by the model. Notably, these isotropic rules predict the emergence of directional bias in the expansion of the ductal network, in the absence of any external guiding signaling gradients. Finally, to challenge the model, we predict, and discover experimentally, novel signatures of the inferred dynamics, which are consistent with an out-of-equilibrium “phase transition”. Moreover, by adjusting experimentally the microenvironment of the branching tips through local or systemic perturbations, we further test the predictive capacity of the model, and gain insight into the molecular regulatory basis of the inferred collective cell dynamics.

Results

Defining the ductal network structure of the mouse mammary gland epithelium

To develop a model of tip-driven ductal morphogenesis, we began by considering the mammary gland epithelium. At birth, the mouse mammary gland is specified as a small rudimentary tree-like structure (Figure S1A). During puberty, precursors localized at ductal tips (termed terminal end-buds) drive the expansion of a complex network through multiple rounds of tip bifurcation and ductal elongation (Sternlicht, 2005) (Figure S1A). These networks are characterized by their non-stereotypicity and structural heterogeneity of their subtrees (which we defined formally as the parts of the ductal tree sharing a common branch ancestor at branch level $l_e = 6$ - which reflects the approximate extent of the rudimentary structure prior to pubertal morphogenesis). Indeed, some ductal subtrees become extremely large, containing as many as 30 generations of consecutive branching events, while neighboring subtrees may terminate precipitously (Scheele et al., 2017).

Recently, we showed through quantitative genetic lineage tracing methods that the complexity of the mammary epithelium does not derive from intrinsic heterogeneity of tip precursor populations, but from the stochastic fate decisions of equipotent tips, which either branch (bifurcate) or terminate (through cell cycle exit) with near equal-probability (Scheele et al., 2017), suggestive of a local control of tip fate. However, such a focus on spatially-averaged models of branching morphogenesis (Zubkov et al., 2015) cannot resolve the spatio-temporal dynamics and mechanistic basis of the underlying regulatory program, nor its potential conservation in other organs.

How can such a balance between tip termination and branching be regulated at the population level? One possibility is that tip branching and termination rates are dependent on the local epithelial density. Indeed, an increase in the termination rate, and/or a decrease in the

branching rate, with local density can ensure that the system reaches a robust steady-state, characterized by a balance between tip branching and termination (Supplemental Text, Section 1.1). Interestingly, such behavior generically produces glands of uniform spatial density (Supplemental Text, Section 1.3), a feature that we verified experimentally by reconstructions of whole adult mammary glands ($n = 14$ glands, Figure 1A,B). However, to understand whether it is branching or termination events that are actively regulated, we turned to quantitative measurements. In particular, parameterization of the distribution of mammary branch lengths (defined as the distance between consecutive branching points) revealed a strikingly exponential dependence, with an average branch length that remains approximately constant over time (Scheele et al., 2017). This observation suggests that the timing between consecutive branching events is random and statistically uncorrelated, pointing to a stochastic and time-invariant program of tip branching. This behavior stands in stark contrast with the early stages of lung morphogenesis, where branch lengths for a given branching level are tightly controlled (Iber and Menshykau, 2013).

We then examined the spatial organization of the ductal network. As the mammary fat pad constrains growth to a thin pancake-like geometry, ductal morphogenesis of the mammary epithelium takes place in a near 2D setting. Against this background, inspection of whole gland reconstructions revealed a strikingly low frequency of ductal crossovers (Figure 1A,C,D and Figure S1) with terminated tips often residing close to an existing duct or the fat pad boundary (Silberstein, 2001). This observation suggests that ductal elongation and branching may proceed as a “default state”, with tip termination occurring only when tips come into proximity with existing ducts. Such behavior is consistent with *in vitro* measurements (Nelson et al., 2006), which show that ductal branching only occurs when remote from the other ducts, with tips that remain close to neighbors remaining inactive.

Mammary morphogenesis proceeds as a branching and annihilating random walk

Interestingly, such a model of branching morphogenesis maps directly onto the theory of “branching and annihilating random walks”, a class of models studied extensively by physicists (Cardy and Täuber, 1996), and showing that the dynamics of binary tip-splitting models converge over time onto a common statistical behavior belonging to the universality class of “directed percolation”. Here, we implemented a minimal model of branching morphogenesis, inspired by the theory of BARWs, where tip dynamics involves only three processes (depicted in Figure 2A):

1. ducts elongate from active tips in a random direction with a speed v - “a persistent random walk” - leaving behind a trail of static, non-proliferative ducts;
2. at any instant, ducts can branch through stochastic tip bifurcation with a constant probability r_b ; and
3. ducts terminate through tip inactivation when tips come within an annihilation radius R_a of an existing duct.

Significantly, numerical simulations of the model dynamics in the absence of physical boundary constraints shows that the system reaches robustly a non-equilibrium steady-state in which the frequency of branching and termination events becomes naturally balanced (Figure S2A,B and Supplemental Text, Section 1.3). As tips are not observed to cross the boundary of the fat pad, and frequently terminate in their proximity (Figure 1A), we further implemented simulations of branching morphogenesis in a rectangular box of length L_x and width L_z to mimic these geometric constraints. Thus, the only key parameter of the model is the ratio between the dimensions of the fat pad and the average branch length l_d (the latter fixed by the ratio v/r_b , Figure 1D). Indeed, this geometrical parameter was fitted to its measured value (Figure S2 and Supplemental Text, Section 1.3.2 and 2.1.2 for details), so that all subsequent comparisons with experiment represent the result of model predictions that do not involve the adjustment of any free parameter.

While a visual inspection of a typical simulation output revealed good qualitative agreement between the experiment and the theoretical predictions of the spatial organization (Figure 2B)

and topology (Figure 2C) of the mammary ductal network, can such a simple model dynamics also provide quantitative insights? To address this question, we first quantified how the predicted frequency of tip bifurcation versus termination events evolves with branch level (i.e. the number of generations since the origin). Interestingly, as well as recapitulating long-term balance in the frequency of tip bifurcation and termination, we found that the model faithfully reproduced the dynamics of convergence towards balance, from an initial stage of symmetric branching early in pubertal development, where the ductal density is low (Figure 2D, $R^2 = 0.73$). Strikingly, the model also predicted with high precision the heterogeneity of subtrees in mammary glands (defined in Figure 2C), quantified both by the subtree size distribution (Figure 2E, $R^2 = 0.96$) and the subtree persistence to a given level (Figure 2F, $R^2 = 0.99$).

Importantly, the spatial model accounted more accurately for the abundance of very large subtrees, which appear due to spatial “priming” in low density regions, than the previously published “zero-dimensional” model (Scheele et al., 2017) in which tip branching and termination events are defined intrinsically and probabilistically (Supplemental Text, Section 3.4). More generally, to explore the specificity of the model, we also considered the quantitative predictions made by eight further classes of models, corresponding to various alternative proposals from the literature. In each case, their applicability to the experimental data was found to be limited (see Figure S3,S4A-D and Supplemental Text, Section 3 for a detailed discussion).

Branching and annihilating random walks reproduce the dynamics of mammary morphogenesis

Having established how the final state of the mammary epithelium is specified, we turned to examine whether the full dynamics of growth could also be predicted quantitatively. To gain insight into the nature and parametric dependences of the growth dynamics, we considered the hydrodynamic limit of the model in which the kinetics is captured by a mean-field theory, a manifestation of a “two-species Fisher-KPP equation” (Fisher, 1937) (Supplemental Text, Section

1.3):

$$\begin{cases} \partial_t a = D\nabla^2 a + r_b a \left(1 - \frac{a+i}{n_0}\right) \\ \partial_t i = r_e i + \frac{r_b}{n_0} a(a+i) \end{cases} \quad (1)$$

where $a(x, t)$ and $i(x, t)$ denote, respectively, the local concentration of active (tip) and inactive (duct) segments or “particles”. Referring to the description of the model dynamics above, active particles diffuse with diffusion constant D while producing inactive segments at rate r_e (reflecting the process of ductal elongation), branch at rate r_b , and annihilate when they meet another particle (reflecting the process of tip inactivation), giving rise to a logistic growth term saturating at a total steady-state density, n_0 . (For details of how Eq. (1) emerges from the stochastic model, and can be related to biological signaling pathways, see Supplemental Text, Sections 1.2 and 1.3). Within this framework, both theory and numerical simulations predict that, during expansion, active tips become self-organized into a narrow pulse at the growing front of the developing epithelium, traveling at constant speed as a solitary wave, and leaving in its wake an inactive ductal network of constant density (Figure 3A,B, Figure S4D-I and Movie S1).

From a biological perspective, this behavior provides a natural explanation for the constant speed of invasion, a robust feature of mammary morphogenesis (Paine et al., 2016). At the same time, the theory predicts that ducts should be patterned at a constant density (Figure 1A,B), while active tips should localize in a predictable pulse-shape distribution at the edge of the invading front. To test these predictions quantitatively, we performed EdU-pulse labeling of mice at 5 weeks-of-age, approximately the mid-point of branching morphogenesis of the mammary gland, and used whole gland reconstruction to both quantify the morphology of the network (Figure 3C and Figure S4J) and define the regional localization of active tips (defined as proliferative tips with $> 50\%$ of EdU+ cells, Figure S4J,K). Importantly, we found good qualitative agreement between experiment and theory, with active tips present at the edge of the growing front and a remarkably constant density of trailing ducts (Figure 3D). Quantitatively, analysis of the spatial profile at the growing front showed that the density of active tips decayed exponentially both

ahead and behind the front, with the decay length of the former larger than the latter by a factor of $(\sqrt{2}-1)$, all key and non-trivial predictions of the Fisher-KPP dynamics (Figure S4F-I and Supplemental Text, Section 1.3.1).

Together, these results suggest that the global spatio-temporal dynamics of mammary ductal morphogenesis can be understood as a process of self-organization following from a program of stochastic tip bifurcation arrested by tip termination at the intersection with neighboring ducts.

Giant density fluctuations and self-organized directional invasion during mammary morphogenesis

Although the proposed mechanism of branching morphogenesis can ensure a uniform density of ducts, statistical fluctuations during growth generate large spatial variations in the distribution of active EdU+ tips (Figure 3C). Indeed, the EdU-pulse assay reveals duct-depleted regions formed either by chance mass termination of tips (Figure S5A) or locally “divergent” flows of active tips randomly exploring other regions (Figure S5B), both behaviors being well-reproduced in the numerical simulations of the model dynamics. Importantly, according to the rules of the model dynamics, the trailing distribution of newly-formed ducts is frozen or “quenched” in the fat pad. Therefore, we expect that the statistical fluctuations of epithelial density should persist in the mature network. Thus, in addition to the prediction of the average density profiles of active tips and mature ducts, the model makes further key quantitative predictions on the statistical properties of spatial density fluctuations.

We thus quantified these fluctuations by defining the spatial average, $\langle n \rangle_L$, and standard deviation, $(\Delta n)_L$, of duct volume in boxes of viable size L (see Figure 4A for a schematic). For systems at equilibrium (in which each elemental process is equilibrated by its reverse, the property of detailed balance), the central limit theorem requires that $(\Delta n)_L = \langle n \rangle_L^\alpha$ with the exponent $\alpha = 1/2$. By contrast, in systems characterized by non-equilibrium fluctuations, α takes values larger than $1/2$ (Ramaswamy et al., 2003; Narayan et al., 2007) - the phenomenon

of giant number fluctuations. Indeed, using the same parameter set as before, model simulations revealed a robust power law dependence of $(\Delta n)_L$ (Figure 4B, green line), with an exponent $\alpha_{\text{theory}} \simeq 0.66$, that increased with decreasing branching rate (Figure S5C).

Turning to previous mammary gland reconstructions at 8 weeks-of-age, we found many instances of large spatial density fluctuations that could not be accounted for by boundary effects, or by the presence of obstacles such as lymph nodes. We therefore applied the same statistical approach to determine experimentally the quantitative dependence of $(\Delta n)_L$ and $\langle n \rangle_L$ ($n = 14$ glands from 7 mice). Strikingly, this analysis revealed a robust power law dependence over more than three orders of magnitude (black dots, Figure 4B), with an exponent of $\alpha_{\text{exp.}} = 0.65 \pm 0.02$ (mean \pm s.e.m), consistent with giant number fluctuations *in vivo*. Moreover, the experimental data collapsed on the theoretical curve with extremely high precision (Figure 4B and Figure S5D), emphasizing the robustness of the model prediction ($R^2 = 0.90$, $R_{\log}^2 = 0.99$). Overall, this analysis uncovers an unexpected out-of-equilibrium feature of branching morphogenesis *in vivo*, and serves as a strong test of the validity and predictive power of the BARW model. In particular, this shows that, while the proposed mechanism enforces (in a self-organized manner), a robust and constant averaged epithelial density, the local density is, as a result, only weakly regulated.

A further ubiquitous feature of mammary gland morphogenesis is the appearance of directional biases in the growth of the ductal network, suggestive of a mechanism that guides tips distally (Figure S5E-J). Indeed, quantification of the distribution of angles θ between a given branch and the horizontal proximal-distal axis (Figure 4C and Figure S5K) revealed a two-fold bias towards a proximal-to-distal orientation (Figure 4D). A puzzle in the field has been the lack of identification of any large-scale gradient which could cause this anisotropy (Gjorevski and Nelson, 2011). However, we reasoned that such a directional bias could derive naturally from the BARW model, even in the absence of global chemical cues or gradients, since branches growing towards the proximal region are more likely to terminate against existing ducts (i.e. less

likely to give rise to progeny), resulting in an “effective” and self-organized bias emerging from isotropic short-range interactions. To test this hypothesis, we computed the theoretical prediction from the same model as above. Strikingly, the model was able to predict quantitatively the experimental profile ($R^2 = 0.95$, Figure 4D), suggesting that directional bias may simply emerge as a natural consequence of the BARW model.

Molecular basis of tip termination and branching

Finally, given the importance of tip annihilation in our framework, we sought to test in a more direct way its underlying molecular basis. Ectopic delivery of TGF- β by large pellets has been shown to reversibly inhibit mammary ductal growth (Silberstein and Daniel, 1987). Therefore, to test the local action of TGF- β signaling, we implanted small TGF- β 1 soaked agarose beads into the mammary fat pads of 4w-old mice, and waited for two weeks before sacrificing the mice (Figure 5A and Supplemental Text, Section 4). Importantly, as predicted by the theoretical simulations (Figure 5A, Figure S5L,M and Supplemental Text, Section 4 for details) and as opposed to experiments with control beads soaked in PBS with 0.1% BSA (Figure 5B and Figure S5N,O), we found that mammary ducts never colonized regions rich in TGF- β 1 beads, while we could observe numerous events of tips having stopped in their close proximity (100 – 200 μ m, blue asterisks on Figure 5A). By contrast, the branching pattern was unaffected in regions devoid of beads (Figure 5A and Figure S5P). These observations support the hypothesis that chemical signaling from maturing ducts regulate the termination of active terminal end-buds and implicate a role for TGF- β 1 in providing the cue in a very local manner.

Next, we wished to assess quantitatively the effect of known positive regulators of branching morphogenesis. We thus performed a similar assay using FGF10-soaked beads (Figure 5C), as FGF10 has been identified as the predominant stromal FGF ligand expressed during pubertal mammary morphogenesis (Zhang et al., 2014). Notably, we found that FGF10 induced a two-fold increase in branching, consistent with its proposed role in driving branch initiation in *in*

vitro studies (Zhang et al., 2014), with a corresponding densification of the network close to beads, which was well-reproduced in model simulations (see Figure 5C and Supplemental Text, Section 4.3 for details).

Together, these two sets of experiments provide both an additional test of the branching and annihilating random walk framework, and a molecular basis for the regulatory program.

Kidney morphogenesis as a 3D branching-annihilating random walk

So far, we have restricted our analysis to the quasi 2D geometry of the mouse mammary gland. Therefore, to address the potential generality of the model to other organs, we considered the 3D incarnation of the BARW model using the development of kidney as a 3D system. During kidney morphogenesis, the ureteric bud, a single outgrowth that arises around embryonic day 11 (E11) from the nephric duct, arborizes to form the collecting system through a repeating process of mainly dichotomous branching. During the course of this iterative branching process, tips induce an aggregate of adjacent cap mesenchyme to undergo a mesenchymal to epithelial transition, thereby initiating the first steps of nephrogenesis, i.e. the formation of nephrons, the kidney's filtration unit. These aggregates continue to mature while the renal connecting tubule concomitantly forms and joins these nascent nephrons with branching collecting ducts (Short et al., 2014; Sampogna et al., 2015; Cebrián et al., 2004). Crucially, as kidney development progresses, a growing subset of older ureteric tips continue to fuse with adjacent maturing nephrons. Once occupied, these tips are thought to no longer contribute to further branching (Sampogna et al., 2015; Costantini and Kopan, 2010), so that they can be considered to have undergone branching termination (Figure 6A).

Motivated by these findings, we thus considered whether the BARW model could predict kidney morphogenesis. Indeed, the convergence of the BARW model towards balanced ductal bifurcation and termination described above is quite general, applying in all dimensions. However, simulating the model dynamics in 3D (Figure 6B,C and Figure S6) revealed that this

convergence, for the same annihilation radius, occurs on much longer time scale (around 3 versus 10 generations, on average, Figure 6D). This behavior can be explained intuitively through differences in the frequency of random collisions between ducts and tips, which become much rarer in 3D as compared to 2D. From a biological perspective, this would mean that the topology of 3D branched organs should appear to be predominantly geometric (deterministic) early in development, displaying serial rounds of symmetric branching events without termination, and only later becoming stochastic in character. Interestingly, such behavior is qualitatively consistent with recent reports by several groups using detailed 3D reconstructions (Short et al., 2014; Sampogna et al., 2015), showing structural heterogeneity and non-stereotypicity only at higher branch levels. We therefore analyzed original and more recent data from (Sampogna et al., 2015), involving kidney reconstructions from E12 to E19, to test whether the same framework could apply during the seemingly non-stereotypical later phase of morphogenesis (Figure 6C and Figure S6).

To develop a more precise quantitative comparison, we considered a numerical simulation of the branching dynamics in an unconfined 3D geometry (Figure S6A-C and Movie S2). In this case, the dynamics depends only on the ratio of the annihilation radius to the characteristic duct length, $R'_a = R_a/l_d$ (Figure S6D-F). In contrast to the 2D setting, this parameter becomes crucial in 3D, where the probability of two branches to cross becomes of measure zero. Moreover, as kidney expands anisotropically, we renormalized all rate constants with respect to growth orientation to match the experimental aspect ratio (Figure S6C and Supplemental Text, Section 5.1).

Interestingly, with $R'_a = 0.25$, a value close to that found for mouse mammary gland, we could reproduce with high precision the growth characteristics of the E19 mouse kidney, as exemplified by the evolution of the tip branching versus termination probability as a function of branch level (Figure 6D). As mentioned above, ductal evolution is characterized by a protracted early phase of symmetric branching, converging slowly towards balanced fate. R'_a is thus the

key and only fitting parameter, and all subsequent comparisons to experiments do not involve the adjustment of any additional parameter.

We then compared the experimental and theoretical topologies of kidneys (Figure 6F), as well as the distributions of branch number as a function of branch level across a wide range of developmental time points (Figure 7A and Figure S6H,I). Given the simplicity of the model, these results showed remarkably good correspondence, revealing an initial phase of geometric ductal expansion (with the number of branches at level n growing as 2^n), followed by a plateauing and widening of the distributions, a manifestation of increasing ductal termination ($R^2 = 0.93$ at E13, $R^2 = 0.95$ at E15, $R^2 = 0.94$ at E17 and $R^2 = 0.93$ at E19, Figure S6I-L). Importantly, this behavior does not arise from purely geometric anisotropies, as can be seen in the same simulation without termination events ($R'_a = 0$) (Figure S6J), or with termination in an isotropic geometry (Figure S7A,B).

Stochasticity in kidney morphogenesis and nephron number specification

In common with the mammary epithelium, growing tips were also predicted to become self-organized into a pulse of activity at the periphery of the developing kidney, while newly-formed nephrons were predicted to form as a secondary pulse behind this front (Figure 6E). Such behavior matched the known organization of the kidney into a nephrogenic zone positioned at the growing periphery of the tissue (Figure S7C) (Sampogna et al., 2015; Short et al., 2014). Moreover, although the time evolution of both the active tip and nephron density can depend on time variations in branching rate, plotting one versus the other provided a robust, time-independent, test of model.

Using glomeruli, the capsule of capillaries located at the beginning of a nephron (Sampogna et al., 2015), as a proxy for the number of maturing nephrons, we found that, after an initial phase of pure tip production without any nephrons, both quantities robustly scaled experimentally, with the relationship well-fit by a power law (Figure 7B and Figure S6K,L). Such scaling

argues for simple time-invariant rules underlying nephron specification, since deviations from this time-invariance would cause deviations from the observed scaling (as simulated in Figure S7D). Crucially, we then compared this observation to our model, using the same parameter set as that used above, and found a good prediction for the scaling relationship throughout the entire time course of embryonic development ($R^2 = 0.78$, $R_{\log}^2 = 0.97$).

To determine whether the model could also predict the detailed heterogeneity of branching structures as well as the averages, we examined the size distributions and persistence of subtrees at each time point (defined as in mammary gland). These were consistently broadly distributed, indicative of large-scale heterogeneity, and adopted similar functional dependences to their mammary counterparts, indicative of conserved (or universal) underlying properties. Crucially, subtree persistences were consistently very well-fit by the model at all developmental time points (Figure 7C, $R^2 = 0.95$ at E13, $R^2 = 0.99$ at E15, $R^2 = 0.97$ at E17 and $R^2 = 0.97$ at E19) as were subtree size distributions (Figure 7D, $R^2 = 0.89$ at E13, $R^2 = 0.99$ at E15, $R^2 = 0.99$ at E17 and $R^2 = 0.93$ at E19).

Finally, although the model captures successfully several non-trivial features of the experimental data, arguing for conserved rules underlying both mammary gland and kidney morphogenesis, we noted that kidney reconstructions were characterized by a rather regular spacing between tips, which was consistently more ordered than the numerical simulations of the model (Figure S6H,I). Indeed, although we found again evidence of giant number fluctuations (Figure 7E), the model slightly overestimated the amplitude of fluctuations (Figure 7E), hinting that tips may be partially self-avoiding, as proposed by (Davies et al., 2014). To incorporate this effect into the model, we proposed that tips, in addition to their persistent random motion, are repulsed by neighboring tips and ducts when within a radius R_r . With v_r defining the characteristic speed change induced by this repulsion, the ratio $f_r = v_r/v$ provides a measure of the strength of the repulsion (Supplemental Text, Section 5.2.5). For large values of f_r , termination becomes extremely rare, yielding a behavior inconsistent with the observed degree of kidney

heterogeneity and nephrogenesis kinetics. However, for small values of $f_r = 0.2$ and a correspondingly larger value of the annihilation radius R_a (Supplemental Text, Section 5.2.5), we could still obtain a satisfactory fit to the data (Figure S6J,L), while obtaining a more ordered kidney structure (Figure S6I). Interestingly, without further adjustment, this improved the fit to the observed density fluctuations ($R^2 = 0.75$, $R_{\log}^2 = 0.98$ Figure 7E).

These findings argue that, although self-avoidance is not the dominant characteristic of kidney morphogenesis (Figure S6M-O), it may cooperate with termination, i.e. nephron maturation, to produce a partially ordered structure. Notably, both elements of the model arise from purely local rules, maintaining the self-organizing character of branching morphogenesis. Indeed, this might explain why it can proceed robustly *in vitro* in the absence of external chemical or morphogen gradients (Davies et al., 2014).

Branching defects as a route to premature termination of branching morphogenesis

Based on these findings, we then questioned their implications for pathologies of branched organs, such as kidney, which have been linked to defects in branching morphogenesis. For instance, hypertension has been proposed to be at least partially explained by insufficient nephron number (Brenner et al., 1988), whereas renal agenesis is a relatively frequent congenital defect in humans, mirroring the *GDNF* knock-out in mice, that results in the formation of tiny rudimentary ductal trees in the kidney (Pichel et al., 1996).

Interestingly, by the stochastic nature of the BARW, chance events may also lead to the premature extinction of active tips, which annihilate against the existing ductal network, inhibiting kidney growth. Although the frequency of such events is negligibly small for the parameters of wild-type tissue (Figure 7F and Figure S7E), higher values of the annihilation radius cause the extinction probability to increase dramatically (Figure 7F, Figure S7F,G and Movie S3).

Numerical simulations reveal a critical point above which early extinction always occurs (Figure 7F and Supplemental Text, Section 5.3), as well as a continuous transition to a non-zero extinction probability below this critical value, which could explain the variable nature of small ductal trees observed in *GDNF* knock-out mice.

Based on this insight, we examined branching morphogenesis on E15.5 littermate kidneys that developed under the condition of mild maternal-fetal Vitamin A-deficiency as described previously (Sampogna et al., 2015). These kidneys are nearly two-times smaller than wild-type (Figure S7H-I), and display larger subtree size heterogeneity ($n = 4$ mice, $P < 0.05$), although the total number of branches remains normal (Sampogna et al., 2015). Noting that Vitamin A deficient kidneys were markedly smaller, we tested whether this measured decrease in branch length was enough to reproduce the enhanced heterogeneity, by producing earlier crowding-induced tip termination (Supplemental Text, Section 6). We found that a uniformly decreased branch length was indeed sufficient to reproduce quantitatively the changes in branch generation distribution in Vitamin A-deficient mice (Figure S7J). Further studies will be needed to address more generically whether such mutant conditions can be understood in terms of ratio between branch length and termination radius, i.e. of their proximity to the annihilating critical point.

Balance between tip termination and branching is also observed in human prostate

Finally, to further explore the generality of the proposed mechanism of branching morphogenesis we turned to consider the human prostate, which consists of independent subunits branching independently from the urethra (McNeal, 1968). Organogenesis of the prostate shares key features of tip driven morphogenesis as described above in breast and kidney formation: The adult branching structure derives from epithelial ductal outgrowths into surrounding urogenital mesenchyme during embryogenesis and the immediate postnatal period (Powers and Marker, 2013).

From the tracing studies of ductal subtrees, based on large-scale 3D reconstructions of adult human prostates ($n = 5$ from 5 patients), some of which extended to 70 generations of branching, we found that some regions terminate early, with tips forming differentiated acini structures, while others grow extensively (Figure S7K). From a plot of the relative probability of tip termination versus branching, we found again that the overwhelming majority of subtrees displayed a striking degree of balance between ductal termination and branching (Figure S7L). Additionally, we found that the functional shape of the distribution was again similar to the other organs, with a few subtrees growing to up to 10 times the average subtree size (Figure S7M). These findings suggest that the paradigm uncovered for mammary gland and kidney morphogenesis may be translated to *a priori* different biological settings.

Discussion

In this study, we have investigated how the branching pattern of the mouse mammary gland epithelium and kidney emerge throughout development. Using a combination of whole-organ 3D reconstruction, proliferation kinetics and biophysical modeling, we have provided evidence that branching morphogenesis proceeds from the spatial competition of equipotent tips, which randomly explore space through a process of ductal elongation and stochastic branching. If this process occurred without competition between growing tips, branched organs would be characterized by stereotypical rounds of purely symmetric branching, with the number of branches increasing with branch level n as 2^n . Indeed, such behavior would serve to minimize the time required to build a branched structure while filling space efficiently. However, reconstructions of mouse mammary gland, kidney and human prostate reveal a different scenario, where tip terminations occur even at the earliest stages of branching morphogenesis, and rapidly balance tip bifurcations at the population level.

Based on the scarcity of ductal crossovers in mammary gland, we propose that the dominant source of tip termination is the presence of neighboring ducts inhibiting growth. This provides a

density-dependent feedback that naturally balances ductal branching and tip termination. This hypothesis challenges the concept of branching morphogenesis occurring through a rigid and deterministic sequence of genetically programmed events, and replaces it by a stochastic self-organizing model of development. After deducing the branching rate from *in vivo* measurements, our model predicts nearly perfectly and without adjustable parameters the network topology and spatial structures of adult mammary glands, while also making a number of additional non-trivial quantitative predictions.

In particular, it predicts the self-organization of active tips into a spatial domain or pulse, localized at the growing front of the network, which invades into the fat pad at constant speed, leaving behind a constant density of mature ducts. As a consequence, our model suggests that the directional invasion of the mammary gland towards the distal end of the fat pad does not need to be guided by a global chemotactic gradient, but instead can be explained quantitatively in a self-organized manner from the short-range annihilating properties of tips and ducts. As a non-equilibrium process, the BARW model predicts quantitatively the existence and scaling dependence of hallmark giant density fluctuations, which we verify experimentally.

Finally, we have shown that the model applies equally well in the 3D setting of the developing mouse kidney, reproducing accurately the network heterogeneity, with some subtrees colonizing large parts of the kidney while others terminate precipitously, as well as the spatio-temporal pattern of nephrogenesis. Such behavior suggests that this self-organized pattern of growth, consistent with the *in vitro* growth capability of kidney trees, may constitute a conserved (universal) mechanism of branching morphogenesis across different tissues, shifting the focus of future studies to the collective spatio-temporal fate control of branching and termination of entire tips, rather than on individual cells.

From a molecular mechanistic perspective, some of the processes underlying tip termination have been studied individually in several organs. In particular, inhibition of tip growth through TGF- β signaling has been demonstrated in both mammary and prostate glands (Silberstein,

2001; Powers and Marker, 2013). $TGF\beta$ is also a good candidate to provide crowding-induced feedback (Silberstein, 2001), as it is known to be diffusible in the stroma, is secreted by mature ducts, and has been shown both *in vitro* and *in vivo* to regulate the branching pattern of pubertal morphogenesis (Silberstein and Daniel, 1987), as confirmed here. Moreover, it was recently reported from *in vitro* culture experiments that the TGF- β superfamily, in particular Bmp7, was also implicated in crossover avoidance in kidney (Davies et al., 2014).

Finally, these findings question the underlying molecular basis of the BARW model. Given the diffusible nature of key underlying regulators, we investigated whether generic reaction-diffusion models could explain the BARW phenomenology. Interestingly, we found that such branching and annihilating dynamics can indeed emerge naturally and robustly from simple Turing-Meinhardt type models (Meinhardt, 1982; Guo et al., 2014) involving only spatial interactions of an activator, an inhibitor and a consumed substrate (Figure S7N and Supplemental Text, Section 7). Taken as a whole, our study demonstrates that the morphogenesis of complex ductal tissues can be understood and predicted quantitatively on the basis of a remarkably simple set of local rules that direct the robust self-organization of a large-scale network structure.

Supplemental information

Supplemental Information includes seven figures and three movies.

Author contributions

E.H, C.L.G.J.S, J.v.R and B.D.S conceived the study and designed the experiments. C.L.G.J.S, M.M., R.H., N.D. and R.S performed experiments and contributed data. E.H, C.L.G.J.S, M.M. and R.S performed analyses. E.H. and B.D.S. developed the theoretical framework. C.L.G.J.S and E.H. made the figures. J.v.R. and B.D.S. supervised the study. All authors discussed results and participated in the preparation of the manuscript.

Acknowledgements

We thank all lab members for helpful discussions, Anko de Graaff and the Hubrecht Imaging Centre for imaging support, and the Hubrecht Institute animal caretakers for animal support. This work was supported by an ERC consolidator grant (648804); research grants from the Dutch Organization of Scientific Research (NWO; 823.02.017), the Dutch Cancer Society (KWF; HUBR 2009-4621), the Association for International Cancer Research (AICR; 13-0297) (all J.v.R), the Wellcome Trust (grant number 110326/Z/15/Z, E.H. 098357/Z/12/Z; BDS), equipment grants (175.010.2007.00 and 834.11.002) from the Dutch Organization of Scientific Research (NWO). EH is funded by a JRF from Trinity College and acknowledges the Bettencourt-Schueller Young Researcher Prize for support. CLGJS is funded by a Boehringer Ingelheim Fonds PhD Fellowship. R.S. was supported by the Norman S. Coplon Extramural Grant.

References

- Brenner, B. M., Garcia, D. L. and Anderson, S. (1988), ‘Glomeruli and blood pressure less of one, more the other?’, *American journal of hypertension* **1**(4 Pt 1), 335–347.
- Cardy, J. and Täuber, U. C. (1996), ‘Theory of branching and annihilating random walks’, *Physical review letters* **77**(23), 4780.
- Cebrian, C., Asai, N., D’Agati, V. and Costantini, F. (2014), ‘The number of fetal nephron progenitor cells limits ureteric branching and adult nephron endowment’, *Cell reports* **7**(1), 127–137.
- Cebrián, C., Borodo, K., Charles, N. and Herzlinger, D. A. (2004), ‘Morphometric index of the developing murine kidney’, *Developmental dynamics* **231**(3), 601–608.
- Costantini, F. and Kopan, R. (2010), ‘Patterning a complex organ: branching morphogenesis and nephron segmentation in kidney development’, *Developmental cell* **18**(5), 698–712.
- Davies, J. A., Hohenstein, P., Chang, C.-H. and Berry, R. (2014), ‘A self-avoidance mechanism in patterning of the urinary collecting duct tree’, *BMC developmental biology* **14**(1), 35.
- Elliott, H., Fischer, R. S., Myers, K. A., Desai, R. A., Gao, L., Chen, C. S., Adelstein, R. S., Waterman, C. M. and Danuser, G. (2015), ‘Myosin ii controls cellular branching morphogenesis and migration in three dimensions by minimizing cell-surface curvature’, *Nature cell biology* **17**(2), 137–147.
- Fisher, R. A. (1937), ‘The wave of advance of advantageous genes’, *Annals of eugenics* **7**(4), 355–369.
- Gjorevski, N. and Nelson, C. M. (2011), ‘Integrated morphodynamic signalling of the mammary gland’, *Nature Reviews Molecular Cell Biology* **12**(9), 581–593.

- Guo, Y., Sun, M., Garfinkel, A. and Zhao, X. (2014), ‘Mechanisms of side branching and tip splitting in a model of branching morphogenesis’, *PloS one* **9**(7), e102718.
- Harrison, L. G. (2010), *The shaping of life: the generation of biological pattern*, Cambridge University Press.
- Hogan, B. L. (1999), ‘Morphogenesis’, *Cell* **96**(2), 225–233.
- Huebner, R. J., Neumann, N. M. and Ewald, A. J. (2016), ‘Mammary epithelial tubes elongate through mapk-dependent coordination of cell migration’, *Development* **143**(6), 983–993.
- Iber, D. and Menshykau, D. (2013), ‘The control of branching morphogenesis’, *Open biology* **3**(9), 130088.
- Kim, H. Y., Pang, M.-F., Varner, V. D., Kojima, L., Miller, E., Radisky, D. C. and Nelson, C. M. (2015), ‘Localized smooth muscle differentiation is essential for epithelial bifurcation during branching morphogenesis of the mammalian lung’, *Developmental cell* **34**(6), 719–726.
- Lu, P. and Werb, Z. (2008), ‘Patterning mechanisms of branched organs’, *Science* **322**(5907), 1506–1509.
- Lubkin, S. R. and Murray, J. (1995), ‘A mechanism for early branching in lung morphogenesis’, *Journal of mathematical biology* **34**(1), 77–94.
- McNeal, J. E. (1968), ‘Regional morphology and pathology of the prostate’, *American journal of clinical pathology* **49**(3), 347–357.
- Meinhardt, H. (1982), *Models of biological pattern formation*, Citeseer.
- Menshykau, D. and Iber, D. (2013), ‘Kidney branching morphogenesis under the control of a ligand–receptor-based turing mechanism’, *Physical biology* **10**(4), 046003.
- Metzger, R. J., Klein, O. D., Martin, G. R. and Krasnow, M. A. (2008), ‘The branching programme of mouse lung development’, *Nature* **453**(7196), 745–750.

- Miura, T. (2008), ‘Modeling lung branching morphogenesis’, *Current topics in developmental biology* **81**, 291–310.
- Narayan, V., Ramaswamy, S. and Menon, N. (2007), ‘Long-lived giant number fluctuations in a swarming granular nematic’, *Science* **317**(5834), 105–108.
- Nelson, C. M., VanDuijn, M. M., Inman, J. L., Fletcher, D. A. and Bissell, M. J. (2006), ‘Tissue geometry determines sites of mammary branching morphogenesis in organotypic cultures’, *Science* **314**(5797), 298–300.
- Paine, I., Chauviere, A., Landua, J., Sreekumar, A., Cristini, V., Rosen, J. and Lewis, M. T. (2016), ‘A geometrically-constrained mathematical model of mammary gland ductal elongation reveals novel cellular dynamics within the terminal end bud’, *PLoS Comput Biol* **12**(4), e1004839.
- Pichel, J. G., Shen, L., Sheng, H. Z., Granholm, A.-C. et al. (1996), ‘Defects in enteric innervation and kidney development in mice lacking *gdnf*’, *Nature* **382**(6586), 73.
- Powers, G. L. and Marker, P. C. (2013), ‘Recent advances in prostate development and links to prostatic diseases’, *Wiley Interdisciplinary Reviews: Systems Biology and Medicine* **5**(2), 243–256.
- Ramaswamy, S., Simha, R. A. and Toner, J. (2003), ‘Active nematics on a substrate: Giant number fluctuations and long-time tails’, *EPL (Europhysics Letters)* **62**(2), 196.
- Riccio, P., Cebrian, C., Zong, H., Hippenmeyer, S. and Costantini, F. (2016), ‘Ret and *etv4* promote directed movements of progenitor cells during renal branching morphogenesis’, *PLoS Biol* **14**(2), e1002382.
- Sampogna, R. V., Schneider, L. and Al-Awqati, Q. (2015), ‘Developmental programming of branching morphogenesis in the kidney’, *Journal of the American Society of Nephrology* **26**(10), 2414–2422.

- Scheele, C. L., Hannezo, E., Muraro, M. J., Zomer, A., Langedijk, N. S., van Oudenaarden, A., Simons, B. D. and van Rheenen, J. (2017), ‘Identity and dynamics of mammary stem cells during branching morphogenesis’, *Nature* **542**(7641), 313–317.
- Short, K. M., Combes, A. N., Lefevre, J., Ju, A. L., Georgas, K. M., Lamberton, T., Cairncross, O., Rumballe, B. A., McMahon, A. P., Hamilton, N. A. et al. (2014), ‘Global quantification of tissue dynamics in the developing mouse kidney’, *Developmental cell* **29**(2), 188–202.
- Silberstein, G. B. (2001), ‘Postnatal mammary gland morphogenesis’, *Microscopy research and technique* **52**(2), 155–162.
- Silberstein, G. B. and Daniel, C. W. (1987), ‘Reversible inhibition of mammary gland growth by transforming growth factor-beta’, *Science* **237**, 291–294.
- Sternlicht, M. D. (2005), ‘Key stages in mammary gland development: the cues that regulate ductal branching morphogenesis’, *Breast Cancer Research* **8**(1), 201.
- Yu, J., Carroll, T. J., Rajagopal, J., Kobayashi, A., Ren, Q. and McMahon, A. P. (2009), ‘A wnt7b-dependent pathway regulates the orientation of epithelial cell division and establishes the cortico-medullary axis of the mammalian kidney’, *Development* **136**(1), 161–171.
- Zhang, X., Martinez, D., Koledova, Z., Qiao, G., Streuli, C. H. and Lu, P. (2014), ‘Fgf ligands of the postnatal mammary stroma regulate distinct aspects of epithelial morphogenesis’, *Development* **141**(17), 3352–3362.
- Zubkov, V., Combes, A., Short, K., Lefevre, J., Hamilton, N., Smyth, I., Little, M. and Byrne, H. (2015), ‘A spatially-averaged mathematical model of kidney branching morphogenesis’, *Journal of theoretical biology* **379**, 24–37.

Figure titles and legends

Figure 1

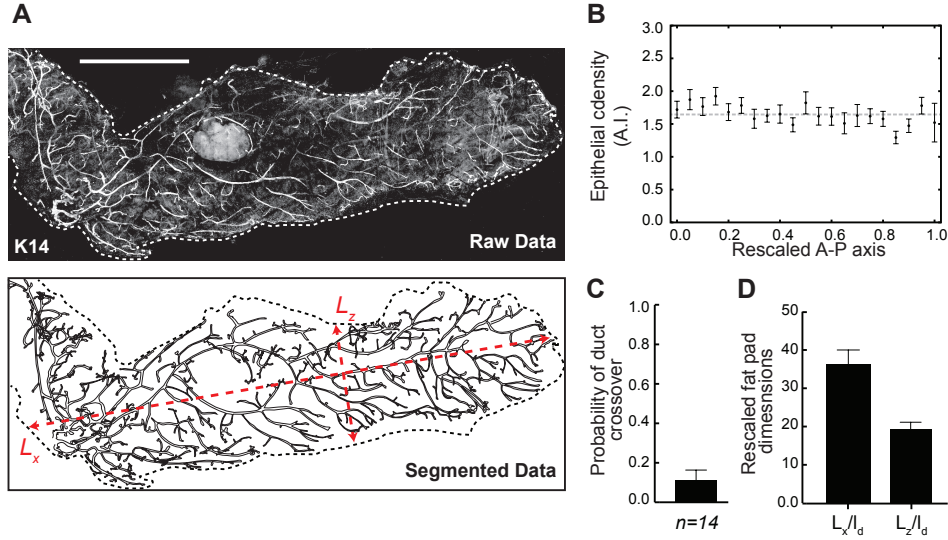


Figure 1: Geometry and characteristics of murine mammary glands revealed by quantitative reconstructions. (A) Quantitative reconstruction (top) and outline (bottom) of a fourth mammary gland based on K14 staining (white), reproduced from (Scheele et al., 2017) along with measurements of the fat pad dimensions L_x and L_z (red). (B) Density profile of ducts along the rescaled antero-posterior axis. (C) Counting of ductal crossovers (normalized by total number of ductal branches) reveal a low crossing probability. (D) Experimentally measured ratio between the dimensions of the mammary fat pad (long axis L_x and short axis L_y) and the average length of a branch l_d , used for the simulations of the mammary gland. Error bars represent mean and s.e.m. Scale bar 5 mm. See also Figure S1.

Figure 2

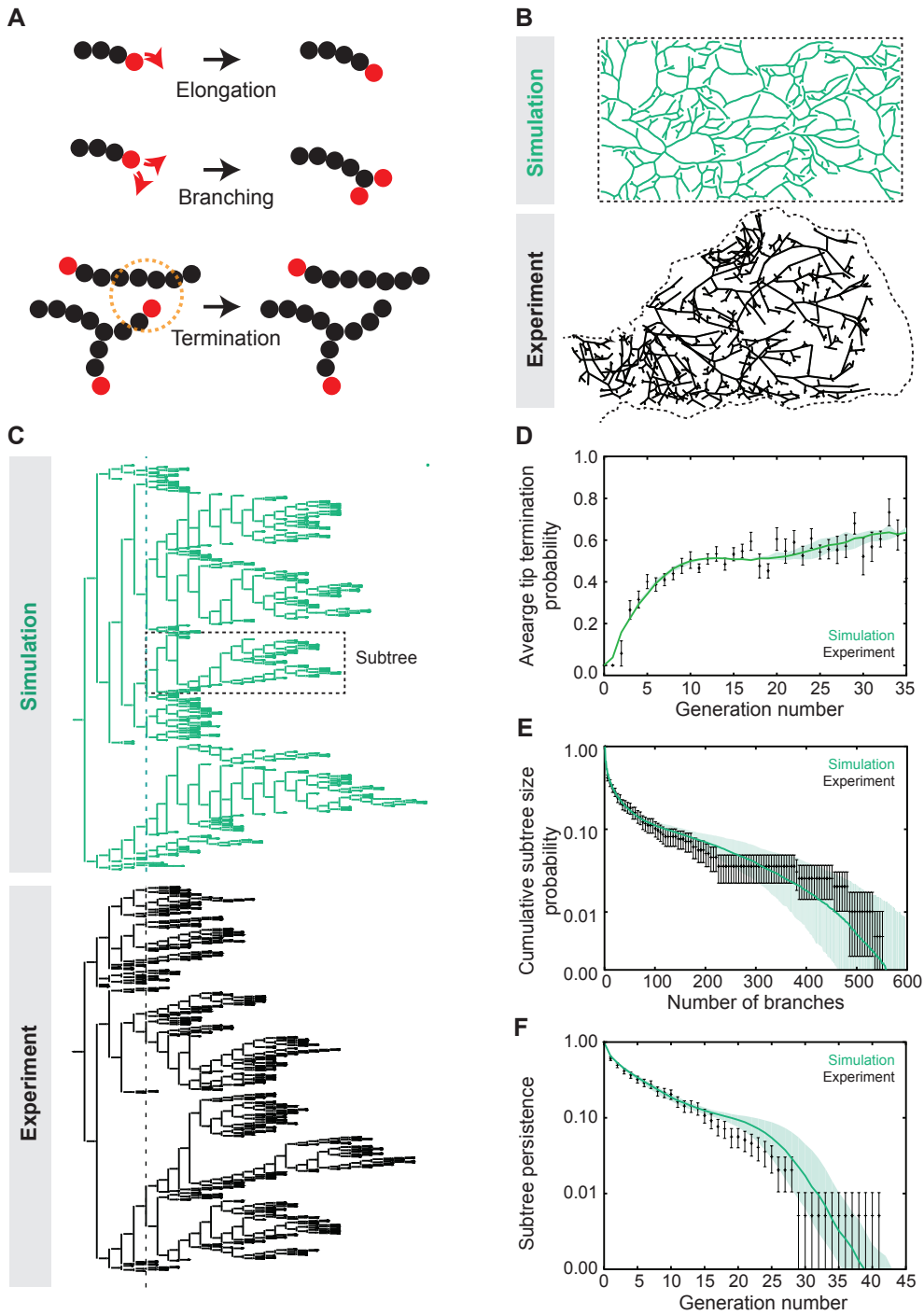


Figure 2: A model based on branching and annihilating random walks predict quantitatively mammary branching morphogenesis. (A) Schematic of the model: Active ductal tips choose between ductal elongation, stochastic branching through tip bifurcation or termination when in proximity to a neighboring duct. (B) Comparison between the experimental and theoretical structure of mammary glands. (C) Comparison between the experimental and theoretical topology of the trees, displaying large heterogeneity, with different subtrees (defined as parts of the tree starting at level 6, delineated as dashed line, with a black box showing an example of a subtree) growing to widely different sizes. (D-F) The BARW model predicts quantitatively the evolution of the probability for tips to terminate (D), the cumulative distribution of subtree size (E), and the subtree persistence to a given branch generation number (F). Data from (Scheele et al., 2017). Shaded area and error bars in (E,F) represent mean \pm one s.d. confidence intervals. Error bars in (D) represent mean and s.e.m. Black represents experiments and green theoretical predictions from simulations. See also Figure S2.

Figure 3

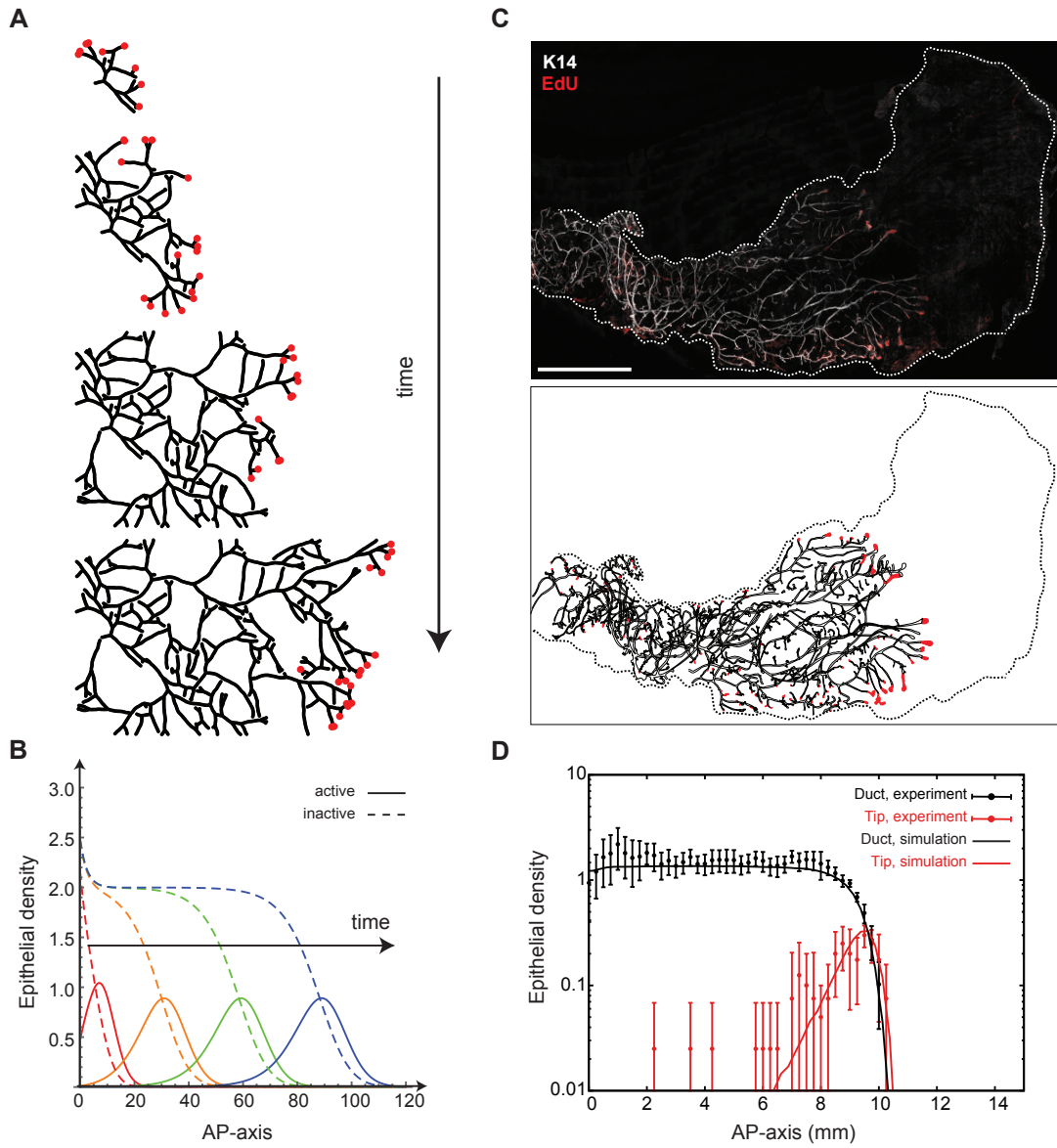


Figure 3: Branching and annihilating random walks reproduce the kinetics of mammary invasion. (A) Numerical simulation of the model at different developmental time points with ducts shown in black and active tips in red. (B) Theory predicts a self-organized solitary pulse of active tips positioned at the growing edge of the network, leaving behind a trail of inactive ducts of constant density. (C) 3D reconstruction of the fourth mammary gland following an EdU pulse at 5w showing the position active tips. Active tips are localized preferentially at the invasion front, mirroring qualitatively the prediction of the model. (D) Density profiles of ducts (black) and fully proliferative tips (red), averaged over $n = 4$ glands, alongside theory (red and black lines, respectively) revealing good quantitative agreement. Error bars represent mean and s.e.m. Scale bar 5 mm. See also Figure S3.

Figure 4

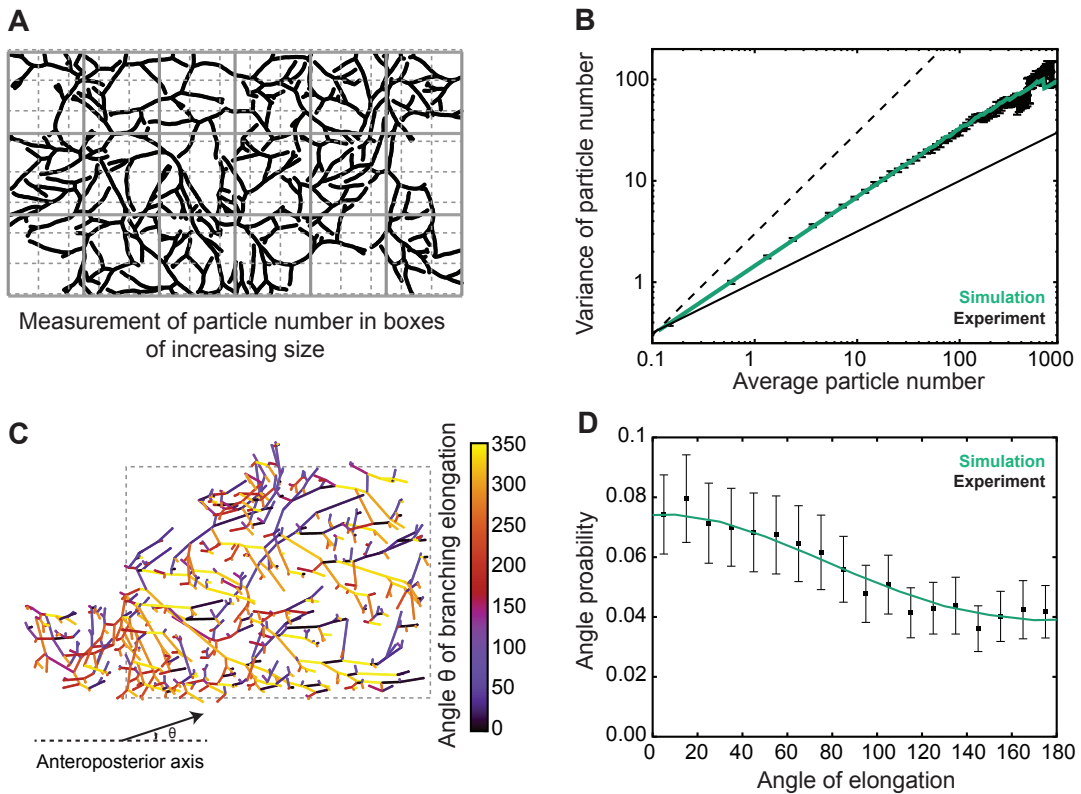
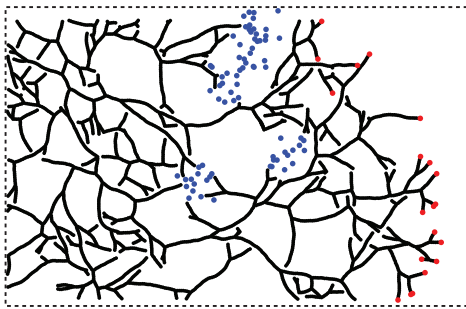


Figure 4: Self-organized properties of BARWs predict both giant density fluctuations and emergent directional bias of ducts. (A,B) Experimental variance (y-axis) versus average (x-axis) of duct volume in boxes of increasing size L (A). The variance in density of the gland at different length scales grows as a power law (B, black bars), with an exponent larger than 0.5 (B, thin and dashed black lines represent exponents of 0.5 and 1, respectively), indicative of giant number fluctuations, and quantitatively predicted by the BARW model (green line). (C,D) Self-organized directional invasion proceeds from local negative interactions: (C) Representative example of the outline of an 8w fourth mammary gland (same as Figure 2B), where the angle θ of each branch segment is calculated relative to the AP-axis; (D) experimental (black bars) and theoretical (green line) distributions showing probabilities of finding a branch growing with a given angle θ . The experimental distribution is predicted quantitatively by the model even in the absence of a large-scale directional gradient. Error bars indicate mean and s.e.m. See also Figure S4 and S5.

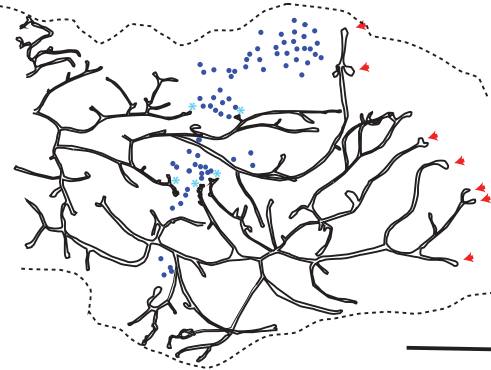
Figure 5

A

TGF- β 1 soaked beads



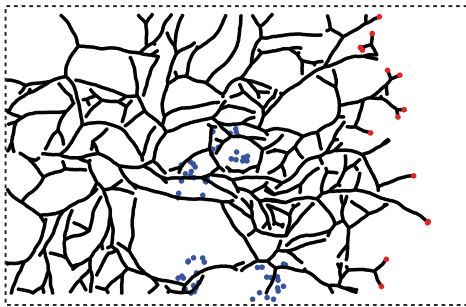
Simulation



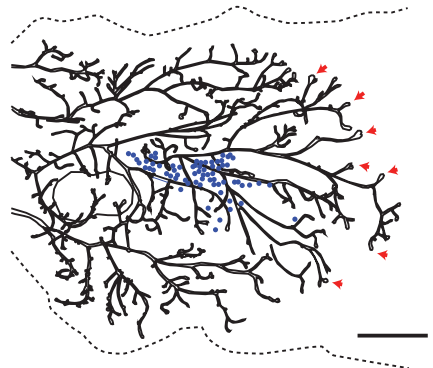
Experiment

B

Control beads



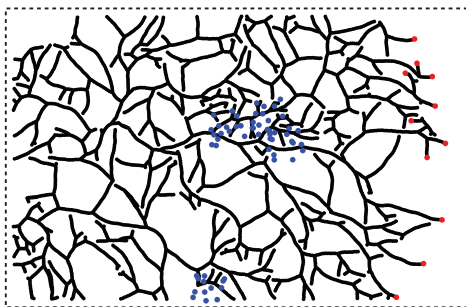
Simulation



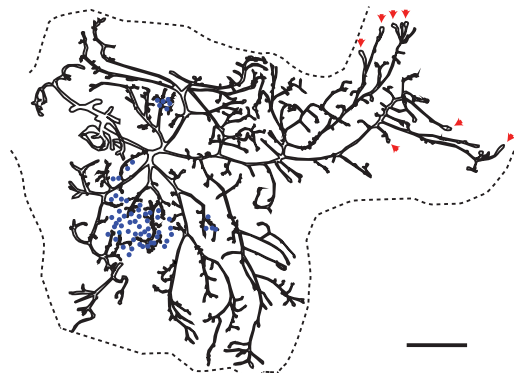
Experiment

C

FGF10 soaked beads



Simulation



Experiment

Figure 5: Perturbation experiments reveal the molecular basis of termination and branching. (A) Comparison between a representative reconstructed fourth mammary gland (right) in the presence of TGF- β 1 soaked beads (blue spheres), and a simulated theoretical counter-part (left). This confirms tip termination in proximity (light blue asterisks) to TGF- β soaked beads. (B) Comparison between a representative reconstructed fourth mammary gland (right) in the presence of control inactive beads soaked in PBS with 0.1% BSA (blue spheres), and a simulated theoretical counter-part (left). Contrary to TGF- β 1 soaked beads, one observes numerous bead-duct overlay. (C) Comparison between a representative reconstructed third mammary gland (left) in the presence of FGF10 soaked beads (blue spheres), and a simulated theoretical counter-part with local two-fold increase in branching rate (right). Active TEBs are marked by red arrowheads. Scale bar 2 mm. See also Figure S5.

Figure 6

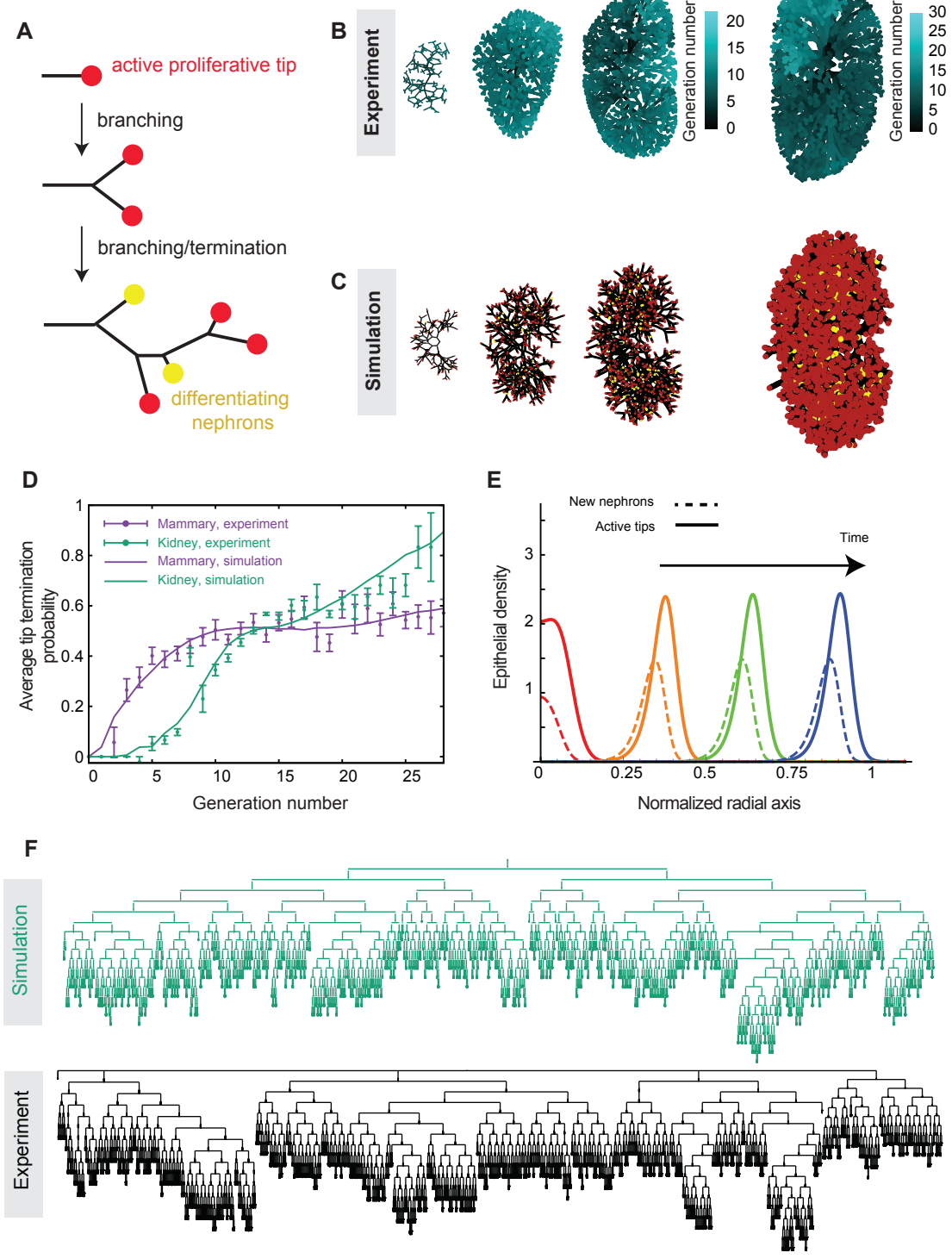


Figure 6: Branching and annihilating random walks can reproduce quantitatively the 3D kidney topology. (A) Schematic of kidney morphogenesis as a stochastic branching process where active tips (red) either elongate, branch or stop contributing to branching via nephron differentiation (yellow). (B) Reconstructions of murine kidney at E13, E15, E16 and E18 (left to right) with generation number of segments color coded in blue. (C) Typical output of numerical simulations of BARW model at corresponding time points. (D) Experimental versus theoretical tip termination probability as a function of generation for mammary gland (purple) and kidney (green), using the radius of termination $R'_a = 0.25$ as the only fitting parameter. (E) The model predicts a self-organized zone of active tips growing at the periphery of the kidney, followed spatially by a domain of tip termination, reminiscent of the nephrogenic zone observed *in vivo*. (F) Tree representation of a E17 kidney branching topology (top, green) and the output of the theory at the corresponding time point (bottom, black). Error bars represent mean and s.e.m. See also Figure S6.

Figure 7

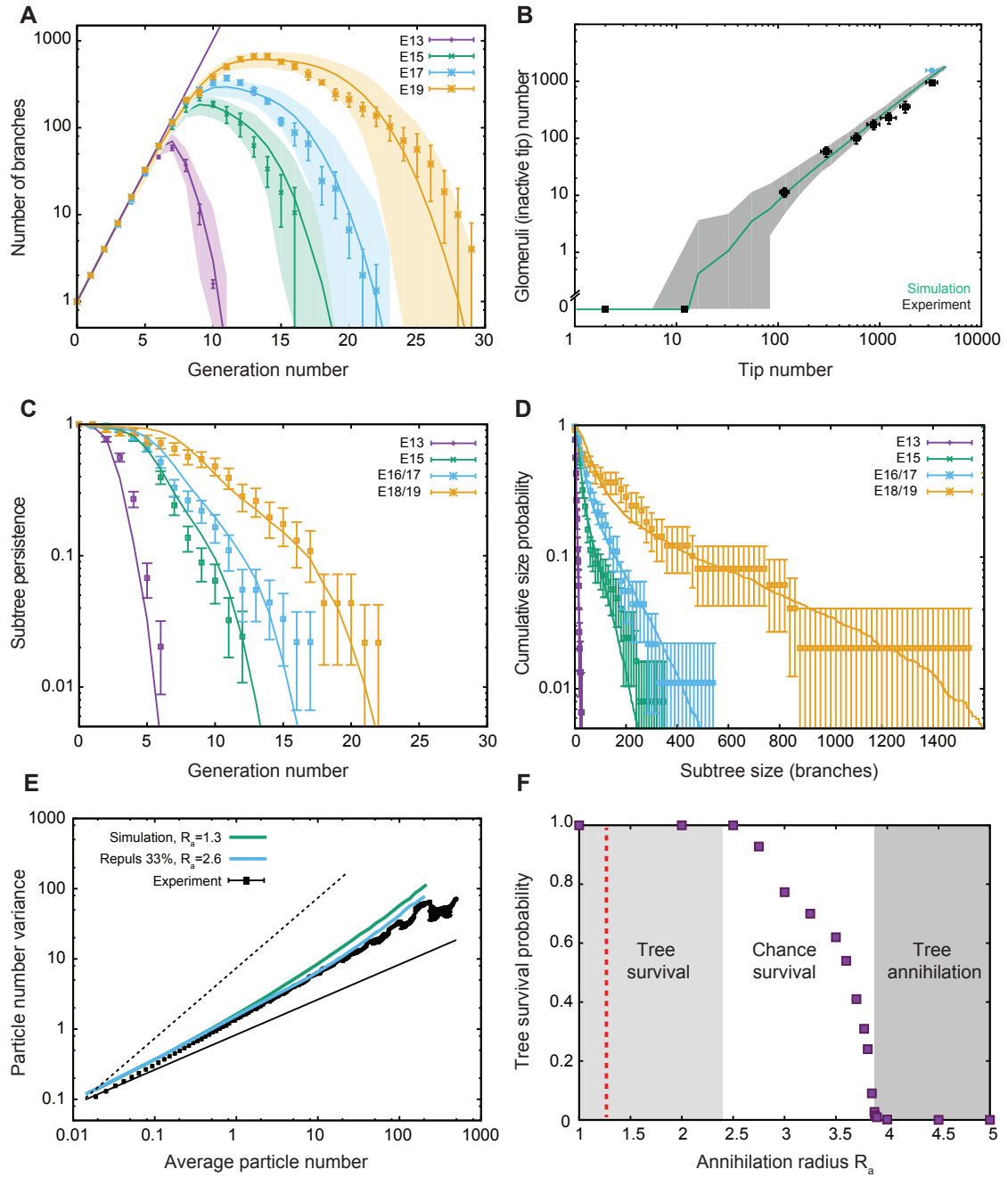


Figure 7: Branching and annihilating random walks can reproduce quantitatively the detailed properties of kidney. (A) Using the radius of termination R'_a as the only free parameter, the model predicts well the number of segments per generation at different time points of embryo development (E13, E15, E17 and E19 in, respectively, purple, green, blue and orange). (B) Inactive tip number (assessed indirectly via glomeruli staining from (Sampogna et al., 2015) in black, or glomeruli counting via a method of acid maturation from (Cebrian et al., 2014) in blue) versus total number of tips, displaying a power law after a phase of purely symmetric branching, predicted by the model (green). (C,D) Experimental distributions of subtree persistence and size at different time points, showing consistently broad distributions which are well-fit by the model. (E) Variance (y-axis) versus the average (x-axis) duct volume in a box of size L (experiments in black) in kidney, showing an exponent larger than 0.5 (thin and dashed black line represent exponents of 0.5 and 1 respectively), indicative of giant number fluctuations. The green and blue lines indicate the prediction from the default model (no repulsion, $R'_a = 0.25$), and a modified model with repulsion ($f_r = 0.33$, $R'_a = 0.5$). (F) Predicted survival probability of kidney morphogenesis vs. termination radius, showing a phase transition above which kidney systematically become fully annihilated. Red dashed line shows the best-fit value of R_a used in A-D. Shaded areas represent 95% confidence intervals and error bars mean and s.e.m. See also Figure S7.